Unraveling oxidation behaviors of MXenes in aqueous systems by Deep Potential Molecular Dynamics Simulations

Pengfei Hou[a], Yumiao Tian[a], Yu Xie[a], Fei Du[a], Gang Chen[a], Aleksandra Vojvodic[b, *], Yury Gogotsi[c, *], Jianzhong Wu[d, *], Xing Meng[a, b, c, *]

[a] Key Laboratory of Physics and Technology for Advanced Batteries (Ministry of Education), College of Physics, Jilin University, Changchun 130012, P. R. China

[b] Department of Chemical and Biomolecular Engineering, University of Pennsylvania, Philadelphia, Pennsylvania 19104, USA

[c] A.J. Drexel Nanomaterials Institute and Department of Materials Science and Engineering, Drexel University, Philadelphia, Pennsylvania 19104, USA

[d] Department of Chemical and Environmental Engineering, University of California, Riverside, California 92521, USA

* Authors to whom any correspondence should be addressed.

E-mail: mengxing@jlu.edu.cn (Xing Meng), jwu@engr.ucr.edu (Jianzhong Wu), gogotsi@drexel.edu (Yury Gogotsi) and alevoj@seas.upenn.edu (Aleksandra Vojvodic).

Abstract

As excellent two-dimensional (2D) materials, MXenes have shown great potential in various fields. However, the degradation of MXenes in humid environments has become a massive obstacle to the further development of MXenes. Among the factors affecting MXenes degradation, water is ubiquitous in preparation and application. However, the oxidation mechanism of MXenes in aqueous environments has not been thoroughly studied. Here we combine the deep neural networks and the iterative concurrent active learning scheme to develop the deep neural network potential of the aqueous MXene system with ab initio precision at the low cost as same as that of the empirical force field. The oxidation behaviors of the super large aqueous MXene system are investigated systematically at nanosecond timescales for the first time. We demonstrate that the degradation of MXenes in aqueous systems, a spontaneous energy minimization process, is indeed caused by water. The proposed proton motion and vanadium oxide protection mechanism effectively explain that the oxidation of MXenes in aqueous solutions is a self-decay process and why MXenes can exist for a relatively long time in aqueous solutions instead of rapid hydrolysis. And the oxidation protection layer, like that of 3D structures, has been seen for the first time from molecular simulations, which may be of guiding significance for studying MXenes protection strategies.

Keywords: MXenes, degradation, deep neural networks, iterative concurrent active learning scheme, oxidation protection layer, proton motion.

Introduction

In the past decade, 2D transition metal carbides, nitrides, and carbonitrides, known as MXenes [1, 2], have the general formula of $M_{n+1}X_nT_x$, where M stands for early transition metals, X stands for C/N, and T_x stands for -F, -O, -OH or other surface groups, and n=1,2,3,4, have great potential in energy storage, [3-6] catalysts, [7-9] sensors, [10-12] electronics [13-15] and other fields [16] due to their excellent properties including hydrophilic surfaces and metallic conductivity.

As typical 2D materials with a high surface area to body mass ratio, MXenes are extremely sensitive to the environment. They often degrade into the corresponding transition metal oxides caused by collective effects from the air, moisture, and light. [17-19] Among these factors, water plays a crucial role in the oxidation process of MXenes, especially for aqueous systems. Early studies have shown that dissolved oxygen in the water caused rapid oxidation of MXene dispersions. [17] However, MXenes also oxidized in water after removing dissolved oxygen, even more, affected by moisture than dissolved oxygen. [20-22] Water is ubiquitous as the most common solvent, [23, 24] and the degradation of MXenes in aqueous solutions destroys the whole structure, which may appear to have unwanted properties, thus seriously damaging the application of MXenes in aqueous systems. The degradation of MXenes in humid environments has become a massive obstacle to the further development of MXenes in various fields. Preventing degradation requires a comprehensive understanding of the oxidation process. However, the oxidation mechanism of MXenes in aqueous environments has not been thoroughly studied. Therefore, to improve the storage and application stability of MXenes, it is urgent to investigate the oxidation mechanism of MXenes meticulously in aqueous solutions at the atomic level.

Molecular dynamics (MD) simulation can restore details of the reactions at the atomic level, which provides a feasible scheme for exploring the oxidation mechanism of MXenes. [25, 26] Owing to the dependence on empirical force fields, the accuracy of classical MD simulation often could not meet the research needs. As a more accurate simulation method based on quantum mechanics, ab initio molecular dynamics (AIMD) simulation has been used to study the MXene-water interface. [27, 28] For example, Jiang et al. studied the proton redox and the hydrolysis of $Ti_3C_2O_2$ in confined water by AIMD simulation. [27, 28] Although AIMD provides accurate insights at the atomic level, there are still a large number of reaction properties and laws ignored due to the limitation on the scale of the materials systems (generally less than 1000 atoms) and the length of the simulation time (usually less than 100 ps), which is hardly sufficient for in-depth exploration of the oxidation process.

Machine learning (ML) methods have made MD with ab initio precision possible at the same low cost as empirical force fields, paving the way for in-depth simulation in large material systems at long-time scales. As the primary ML method, theoretically speaking, deep neural network potential (NNP) based ab initio data could be infinitely close to the precision of the data. [29, 30] NNP has been successfully used in multi/single-element bulk, aqueous, and other complex systems.[31-33] NNP could solve the above problems caused by the low accuracy of the empirical force field and the high cost of AIMD, thus making it possible to study the oxidation process of MXenes in aqueous systems accurately.

Here, we combine deep neural networks and the iterative concurrent active learning scheme [31, 34] to develop the NNP of the V_2CO_2-H_2O system. And then, the oxidation reaction process on the

V_2CO_2-H_2O interface is investigated comprehensively by deep potential molecular dynamics (DPMD). Surprisingly, the oxidation rate of V_2CO_2 in water decays rapidly in nanosecond MD simulations and decreases with the increase of water layer thickness. And then, we propose proton motion and vanadium oxide protection mechanisms to explain these fascinating phenomena. Our study provides theoretical guidance for illustrating the hydrolysis mechanism of MXenes and enhancing the storage and application stability of MXenes.

Results

The NNP training process. Considering the interaction between V_2CO_2 and different water layer thicknesses, the initial NNPs are built from all configurations of $V_{24}C_{12}O_{24}$-10/20/30/40H_2O, which are equal time interval structures by AIMD with canonical (NVT) ensemble. And then, the NNPs are used by the Deep Potential Generator (DP-GEN) to explore the broader region of the phase space with isothermal-isobaric (NPT) DPMD trajectories. Temperatures are analyzed from 250 K to 350 K, and pressures are from 0.5 bar to 1.5 bar. The exploration begins with V_2CO_2-H_2O structures relaxed by DFT, as shown in Figure S1. To include the oxidation state configurations in the NNPs, the exploration time for each model ranges from 500 fs to 100000 fs. This ensures that the NNPs could accurately describe the oxidation process. The iterative concurrent learning scheme executed by DP-GEN consists of three stages, training, exploration, and labeling. In the training stage, four NNPs are constructed based on the same training dataset but with random initialization parameters. During the exploration process, several DPMD simulations are performed with a set of thermodynamic conditions on different V_2CO_2-H_2O structures by four NNPs. For each V_2CO_2-H_2O configuration, the difference is estimated by the

maximal deviation of the forces (σ_f^{max}) predicted by four NNPs. In the labeling process, the configuration will be labeled to get the relative energy and force through DFT calculations when $\sigma_{lo} \leqslant \sigma_f^{max} < \sigma_{hi}$, where σ_{lo} and σ_{hi} are respectively lower and upper trust levels adjusted by users. In this work, σ_{lo} and σ_{hi} are set to 0.12 eV/Å and 0.36 eV/Å, which is accurate enough for the aqueous systems. [32, 35] The new data will be added to the original dataset for subsequent exploration learning. The whole process of developing NNPs is shown in Figure 1. After 38 iterative concurrent learning, the exploration of V_2CO_2-H_2O systems is considered converged when the percentage of accurate configurations is larger than 99%. The final dataset includes 11921 structures, a tiny fraction (0.017%) of the configurations explored by DPMD. Finally, we have acquired an NNP of V_2CO_2-H_2O systems through 8 million training steps by DeePMD-kit. [36]

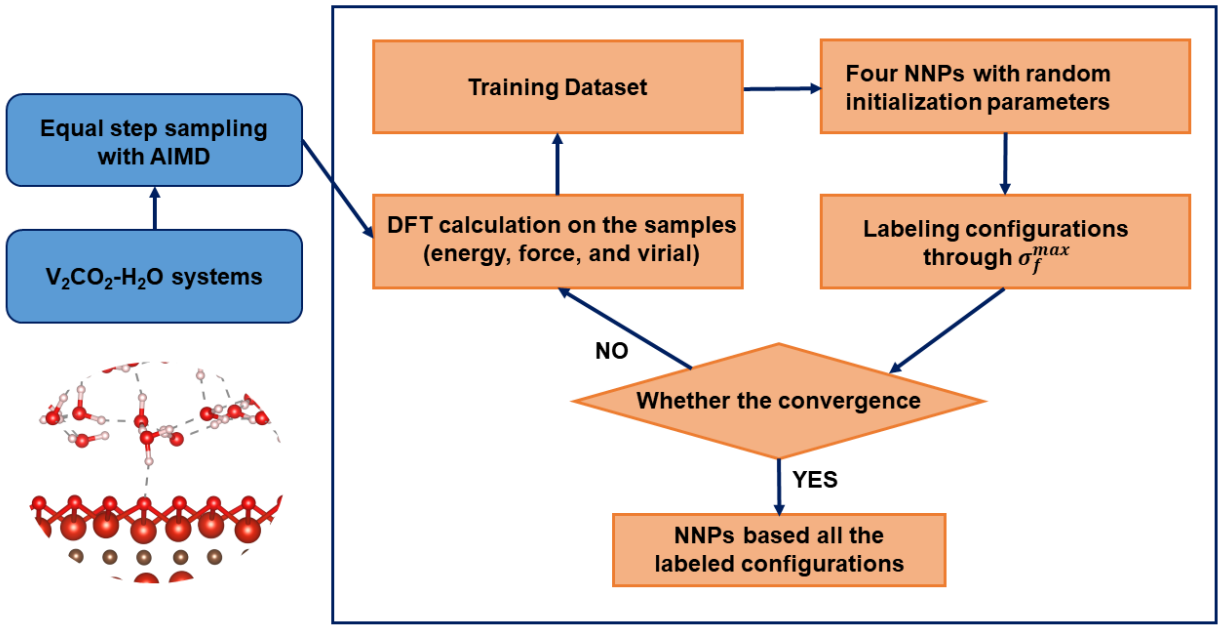

Figure1. The whole process of developing NNPs for V_2CO_2-H_2O systems.

The accuracy of the NNP for V_2CO_2-H_2O systems. The errors of the NNP relative to DFT are quantified by energy and force independence tests based on a series of V_2CO_2-H_2O MD trajectories (1579 configurations) that are different from the training dataset. The root mean square errors (RMSE) of energy and force are 2.35 meV/atom and 0.083 eV/Å, respectively. The diagnostic plots between DFT and NNPs and energy RMSE distribution are shown in Figure S2. To verify the accuracy of the NNP in simulating the properties of V_2CO_2-H_2O systems, we compare the pair correlation function and vibrational density of states for different water layer thicknesses by AIMD and DPMD. As shown in Figure S3, it can be seen that the NNP shows surprising consistency with AIMD in the treatment of V_2CO_2-H_2O systems.

The vanadium oxide formed on the surface of V_2CO_2. Experimentally, the interlayer distance of MXenes could change with water intercalated between layers. As shown in Figure S4, the optimal interlayer spacing is determined for V_2CO_2-H_2O systems, including different water layer thicknesses (10 H_2O, 20 H_2O, and 30 H_2O). And then, we performed 10ns DPMD with NVT ensemble using the trained NNP to observe the long-term oxidation behaviors of V_2CO_2-H_2O systems at room temperature (300 K). The final snapshots are shown in Figure 2. There are vanadium oxides on the surface of V_2CO_2 for different V_2CO_2-H_2O systems. As shown in Figure 2 (d), a vanadium oxide consists of a V atom, three surface O groups, and an O atom from water, which exhibits the tetrahedral configuration. And Table S1 shows that the V-O bond strength of the vanadium oxides on the surface is stronger than that of most common vanadium oxides, which proves the relative stability of the surface vanadium oxides. To observe the formation time of the

vanadium oxides and the effect on the stability of the systems, energy-time plots and the minimum distance between V atoms and O atoms in water are shown in Figure S5. V_2CO_2-H_2O systems become more stable with the decrease (about 2-3 eV) in energy when the formation of vanadium oxides, which indicates the degradation of MXenes is an energy minimization process. More surprisingly, the formation time of the vanadium oxides will push backward with the increase of the water layer thickness, and two vanadium oxides form on the surface of the 10 H_2O system for which the first vanadium oxide appears earliest. In the early MD simulation, the minimum distance between the V atom and the O atom in water is about 3.55 Å, which gets close to the sum (3.60 Å) of van der Waals radii of V and O shows the water molecules physically adsorb on the V atoms. [37] After oxide formation, the minimum distance is 1.61 Å, standing for the strong covalent interaction [38], and remains stable during 10 ns MD simulation. The appearance of vanadium oxide is a spontaneous transition from physical to chemical adsorption. The formation of surface vanadium oxides, a spontaneous process, could improve the stability of the MXenes in aqueous systems. This explains why MXenes are easy to degrade in the aqueous environment.

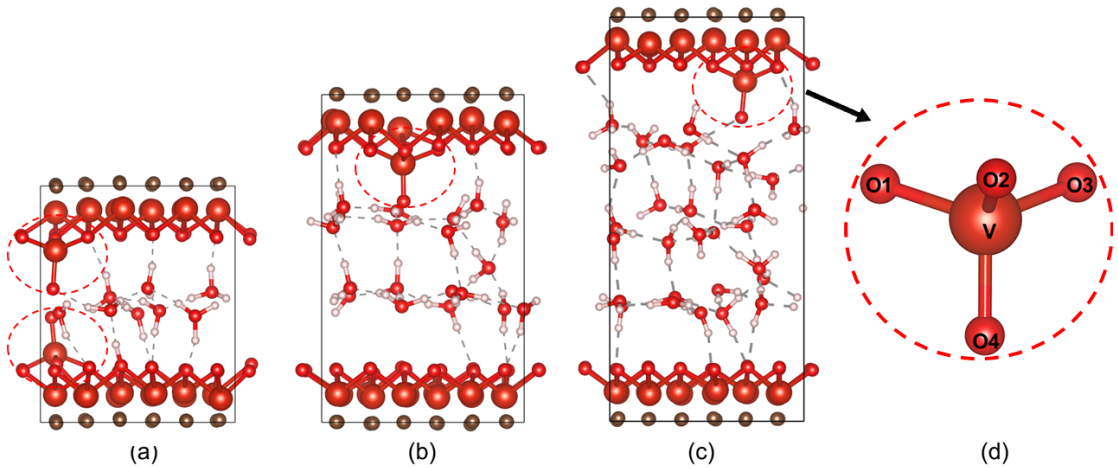

Figure 2. The final snapshots for V_2CO_2-H_2O systems with (a) $10H_2O$, (b) $20H_2O$, and (c) $30H_2O$. (d) The local magnification of the vanadium oxides.

The oxidation process at the atomic level. Understanding the oxidation mechanism is the most critical strategy for studying the degradation of MXenes. As shown in Figure 3, the whole process could be roughly divided into two stages, water molecule adsorption on the V atom and the protons released. In the first stage, the O atom in the H_2O is oriented toward the V_2CO_2 surface, and the V atom is pulled out of the equilibrium position, forming a V-O bond at the end of the first stage. And then, with the aid of the two nearest H_2O, the two O-H bonds break one by one along with the decrease of the V-O bond distance, resulting in the formation of the stable vanadium oxide on the surface. The changes in bond lengths among related atoms are shown in Figure 3 (c) during the oxidation process, showing the precise surface oxidation mechanism. To make sure the accuracy of the NNP in simulating the oxidation states, the energy of the oxidation intermediate state is calculated by DFT and compared with the potential energy predicted by DPMD. As shown in Figure 3 (d), the energy prediction of the NNP is almost the same as that of DFT for the oxidation states, which proves the effectiveness of the NNP for oxidation process simulation. Therefore, we then extended the NNP to study the super large V_2CO_2-H_2O systems.

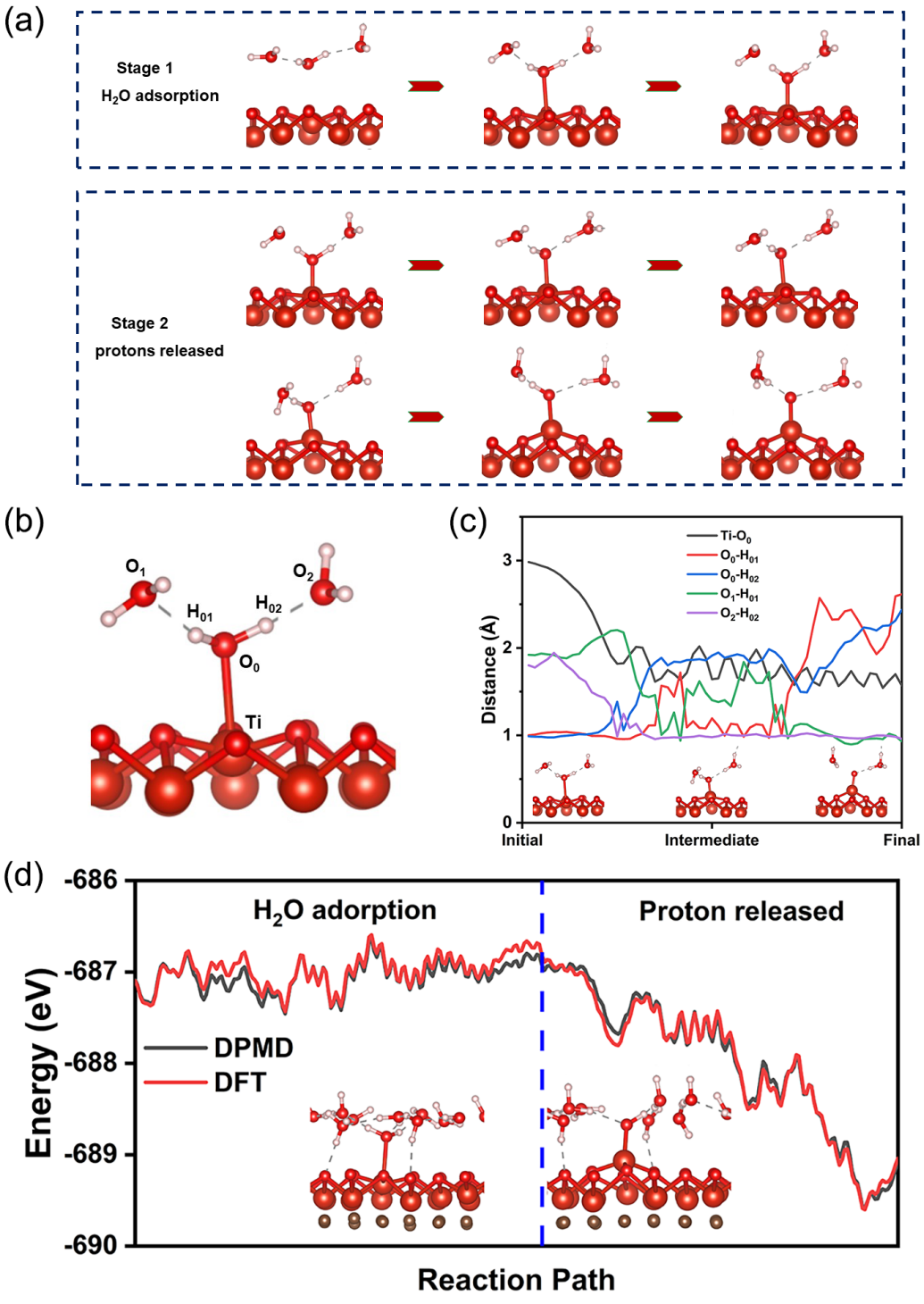

Figure 3. (a) The oxidation process in V_2CO_2-H_2O systems. (b) Oxidation transition state structure. (c) The changes of bond lengths among related atoms. (d) The energy of the oxidation transition states is calculated by DFT and DPMD.

Oxidation behaviors for super large V_2CO_2-H_2O systems. In the past, the super large aqueous MXene systems (more than thousands of atoms) that could provide more oxidation reaction information, such as oxidation rate, have never been explored due to the limitation of the simulation method. Here, we have performed the MD simulation of the super large V_2CO_2-H_2O systems, including different water layer thicknesses (1000 H_2O, 2000 H_2O, 3000 H_2O) by using 10×10×1 supercell structures that contain 2400 V atoms at room temperature (300 K) with NVT ensemble, and the final snapshots are shown in Figure S6. The relationship between the amount of vanadium oxide formation and the simulation time is shown in Figure 4 (a). The simulation process is divided into two stages, the speediness stage (0 ps ~ 200 ps) and the saturation stage (200 ps ~ 1000 ps).

The effect of water layer thickness on oxidation rate. During the speediness stage, the vanadium oxide formation rate decreases significantly with the increase of water layer thickness, which is an interesting phenomenon to explore further. As shown in Figure 4 (b), the average minimum distance between the stable V atoms (defined as V atoms that have not formed vanadium oxides) and the O atoms in water ($(V\text{-}O)_{average}$ distance) increases as the increase of water layer thickness due to the hydrogen bond network formed among the water molecules. Figure 4 (c) shows the distribution of hydrogen bonds for different water layer thicknesses. There are no hydrogen bonds in the vertical direction for one water layer, which causes the water molecules to move freely in the vertical direction, leading to the smallest $(V\text{-}O)_{average}$ distance. And then, more and more vertical hydrogen bonds limited the vertical movement of the water molecules, thus making the

$(V\text{-}O)_{average}$ distance longer with the increase of water layer thickness. The shorter $(V\text{-}O)_{average}$ distance promoted the formation of vanadium oxide. Therefore, the vanadium oxide formation rate increased significantly with the decrease of water layer thickness during the speediness stage.

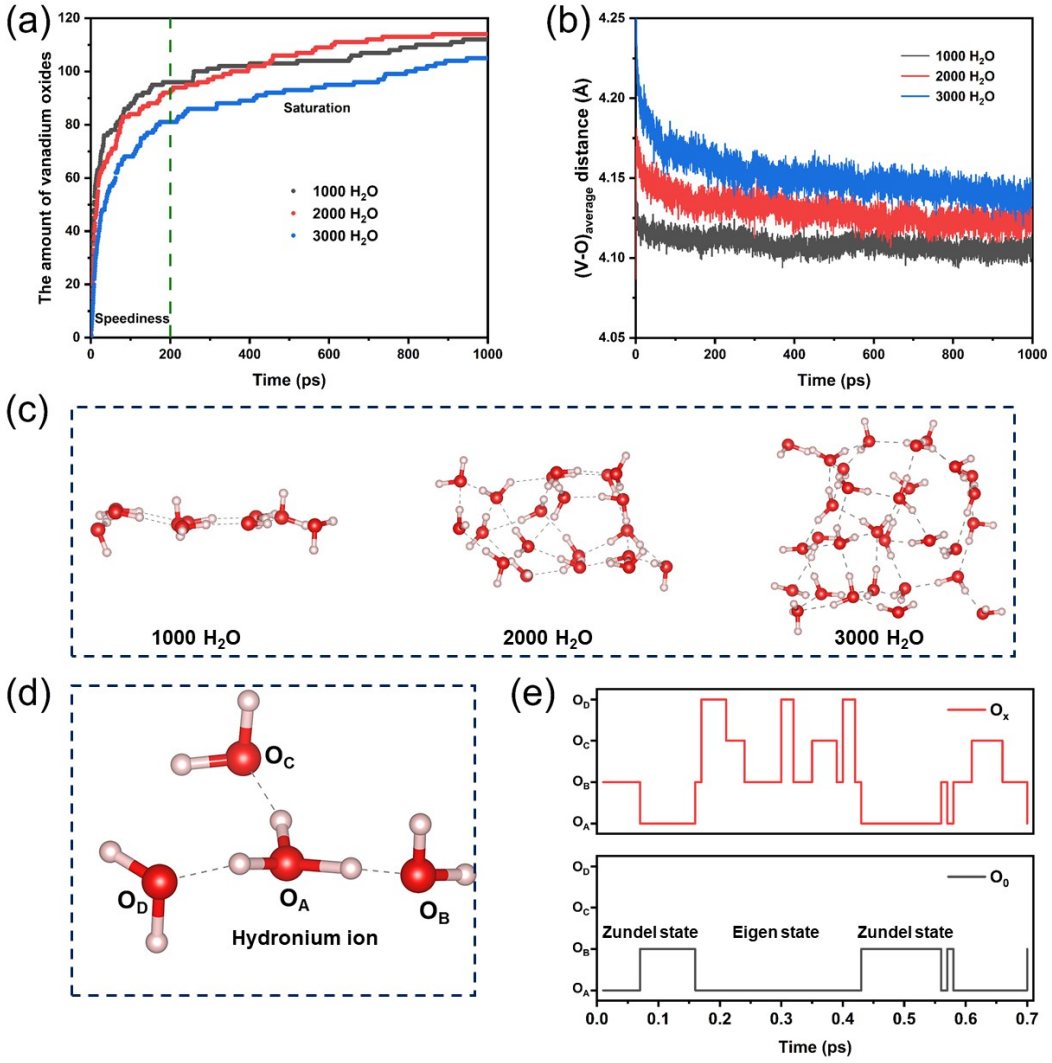

Figure 4. (a) The relationship between the number of vanadium oxides and the simulation time. (b) The average minimum distance between the stable V atoms and the O atoms in water. (c) Local hydrogen bond networks for V_2CO_2-H_2O systems, including 1000 H_2O, 2000 H_2O, and 3000 H_2O. (d) The typical coordination environment for a hydronium ion in water. (e) O0 and Ox identity

change among O_A, O_B, O_C, and O_D.

During the saturation stage, the vanadium oxide amount of the 2000 H_2O system exceeded that of the 1000 H_2O system at about 400 ps, which is attributed to the binding effect between protons and water molecules. It can be seen that the formation of vanadium oxides relies on the oxygen atoms from water molecule cleavage, leading to two free protons that exist as hydronium ions in water. Figure 4 (d) shows the typical coordination environment for hydronium ions in water. We define the O atom in the hydronium ion as O_0 and its nearest O atom as O_x. The change of O_0 and O_x identity represents the motion of the proton in water. The change of O_0 and O_x identity is shown in Figure 4 (e). The proton motion process can be divided into two states: the Eigen state and the Zundel state. [27, 39] For the Zundel state, the proton is shared by O_A and O_B. That is, O_0 and O_x identities only switch between O_A and O_B. During the Eigen state, the proton is captured by O_A and O_x switches among three adjacent oxygen atoms, O_B, O_C, and O_D. The motion of protons in V_2CO_2-H_2O systems follows the Eigen-Zundel-Eigen mechanism as in bulk water. The four water molecules used for proton transport could not participate in the oxidation reaction. The formation of a vanadium oxide results in two free protons that restrict the movement of eight water molecules. The 1000 H_2O system gradually reached the saturation state (nearly 100 vanadium oxides at 400 ps) with the increase of the restricted water molecules (theoretically restricted 800 water molecules at 400 ps), which slowed the oxidation reaction rate. Therefore, it is normal that the vanadium oxides amount of the 2000 H_2O system exceed that of the 1000 H_2O system at about 400 ps.

The vanadium oxide protection mechanism. Based on the above analysis, the 2000 H_2O and

3000 H_2O systems should have enough water molecules to continue the oxidation reaction. That is not the case. The vanadium oxide formation rate decreased significantly with the increase of simulation time for all V_2CO_2-H_2O systems, behind which there must be a deeper reason. We have extracted the local model from the super large 3000 H_2O system and considered the distribution position of vanadium oxides. As shown in Figure 5 (a), it can be seen that the distribution of vanadium oxides is very scattered, and the adjacent V atoms do not become vanadium oxides at the same time. Besides, as shown in Figure 5 (b), the outermost O atom of vanadium oxides can form hydrogen bonds with two water molecules. And there is a vacuum area underneath the two water molecules. Therefore, we assume that the presence of the vanadium oxides could create protective layers with the surrounding water molecules, thus protecting the nearest vanadium atoms from the attack of other water molecules, namely the vanadium oxide protection mechanism. The six closest V atoms around each vanadium oxide are defined as the protected V atoms. The average minimum distance between V atoms and O atoms in water and the probability of H_2O physical adsorption (the V-O distance is less than 3.60 Å) on V atoms for the protected and the stable V atoms are shown in Figures 5 (c) and (d). The $(V\text{-}O)_{average}$ distance of the protected vanadium atoms is larger than that of the stable vanadium atoms, and the probability of H_2O physical adsorption of the protected vanadium atoms is less than that of the stable vanadium atoms, which together support the hypothesis of the vanadium oxide protection mechanism. As shown in Figure S7, the $(V\text{-}O)_{average}$ distance and the probability of H_2O physical adsorption also offer the same pattern for the 1000 H_2O system and the 2000 H_2O system.

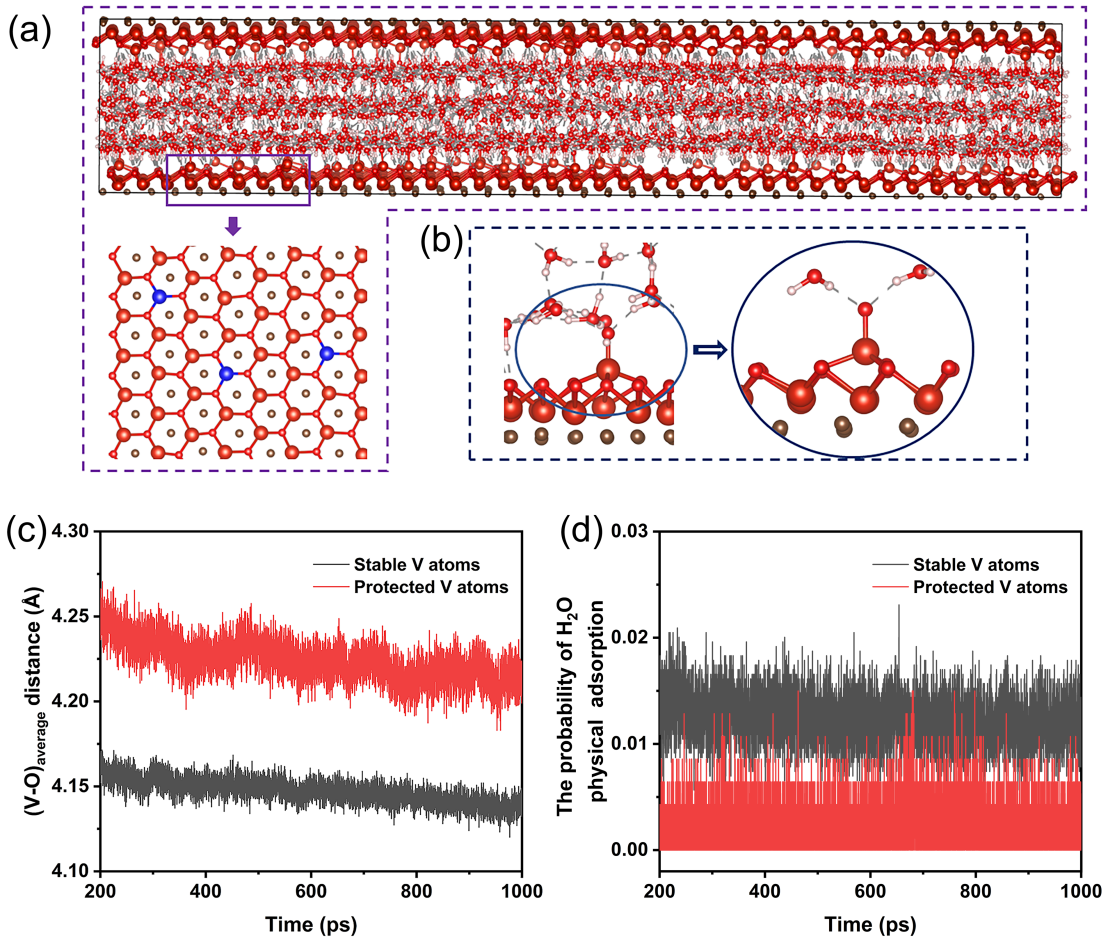

Figure 5. (a) The distribution position of vanadium oxides (blue atoms). (b) The vanadium oxides with water molecules. (c) The average minimum bond lengths between vanadium and oxygen atoms in water, and (d) the probability of H_2O physical adsorption for the protected and stable vanadium atoms.

Discussion

Taking V_2CO_2 as an example, the detailed oxidation process of MXenes has been presented in aqueous systems. When MXenes encounter the aqueous solutions, the oxidation reaction will spontaneously take place with the aid of water, which reduces the energy of the whole system and

produces stable transition metal oxides. During the speediness stage, the oxidation rate decreases significantly with the increase of water layer thickness owing to the restricted motion of water molecules by hydrogen bond networks in the vertical direction. And then, as the oxidation process develops, the movement of the free protons from water cleavage restricts more and more water molecules not to participate in the oxidation reaction. Therefore, the system, including fewer water molecules, saturates first. Besides, during the oxidation process, the oxides could form protective layers with the adjacent water molecules, thus preventing other water from attacking the adjacent transition metal atoms, further inhibiting the oxidation rate. MXenes will be converted entirely to the relative transition metal oxides in a short time if the initial oxidation rate is maintained. The proposed proton motion and oxide protection mechanism explains why MXenes could be preserved in water for a relatively long time. [17] Besides, to some extent, the discovery of the oxide protection mechanism also explains the decay of the oxidation rate of MXenes with time in humid environments. [21, 40, 41]

Though we have studied the long-term oxidation behaviors of the super large MXenes aqueous systems based on NNP, many factors still affect the oxidation process of MXenes to be explored. Recently, inorganic salts can improve the stability of MXenes in aqueous solutions. [42] And the natural MXenes systems often contain vacancies and mixed functional groups such as -F, -OH, and -O. [16] Besides, oxygen also plays a vital role in the oxidation process. [19] In the past, it has been challenging to account for these complex factors in computational simulations fully. Nowadays, the perfect NNP containing more complete data could get more rules of the oxidation behaviors, which opens a promising way to investigate MXenes degradation.

In this work, we develop the NNP of V_2CO_2-H_2O systems in this work using deep neural networks and the iterative concurrent active learning scheme. The oxidation behaviors of the super large MXenes aqueous system are investigated systematically. A detailed and clear picture of the oxidation process between water and MXenes has been shown for the first time. We demonstrate that the degradation of MXenes in aqueous systems, a spontaneous energy minimization process, is indeed caused by water. For the first time at the atomic level, the proton motion and vanadium oxide protection mechanism explain that the oxidation of MXenes in aqueous solutions is a self-decay process and why MXenes could exist for a relatively long time in aqueous solutions instead of rapid hydrolysis. And the oxidation protection layer, like that of 3D structures, has been seen for the first time from molecular simulations, which may be of guiding significance for studying the MXenes degradation mechanism. With the aid of machine learning, the revelation of the MXenes degradation behaviors promotes the development of synthesis strategies for high chemical stable MXenes, thus driving the booming development of MXenes in all fields.

DFT setup

DFT calculations were performed using the projector augmented wave (PAW) [43] method applied in the Vienna Ab Initio Simulation Package (VASP). [44] The exchange-correlation effect was expressed through the generalized gradient approximation (GGA) of the Perdew–Burke–Emzerhof (PBE) method. [45] Grimme's D3 method was employed to make vdW corrections for V_2CO_2-H_2O systems. [46, 47] The cut-off energy was set to 450 eV for the plane-wave basis set. The energy convergence criterion was 10^{-6} eV. The k-points grid of $2 \times 2 \times 2$ and $2 \times 2 \times 1$ with a

Monkhorst-Pack scheme was adopted for $V_{24}C_{12}O_{24}$-10/20H_2O (90 and 120 atoms) and $V_{24}C_{12}O_{24}$-30/40H_2O (150 and 180 atoms).

DeePMD-kit setup

The NNPs were trained and connected with LAMMPS [48] by the DeePMD-kit. [36] The size of the embedding net was (25, 50, 100), and the size of the fitting net was (240, 240, 240). The cut-off radius was 6 Å. The smoothing parameter rcut_smth was set to 0.5 Å. The prefactors of the energy, the force, and the virial terms in the loss functions changed from 0.02 to 2, from 1000 to 1, and from 0.01 to 0.1 during the optimization process. The starting learning rate was 0.001 and exponentially decayed to 10^{-8} at the end of the training.

Supporting Information

Supporting Information: Additional figures as mentioned in the text. Supporting information is available from the authors.

Conflict of Interest

The authors declare no conflict of interest.

Funding Sources

The National Natural Science Foundation of China (Grant No. 12022408) and the Department of Science and Technology of Jilin Province of China (Grant No. 20220402016GH).

Acknowledgments

This work was supported by the National Natural Science Foundation of China (Grant No. 12022408) and the Department of Science and Technology of Jilin Province of China (Grant No. 20220402016GH). All DFT calculations were carried out at the High-Performance Computing Center of Jilin University, China. The NNPs training and MD simulation were performed on two NVIDIA A100 cards at the National Supercomputer Center in Tianjin, China. We thank Paul Kent, John Wang, Musen Zhou, Teng Zhang, Robert Lord, Meikang Han, and Danzhen Zhang for helpful discussions and technical support.

References

[1] M. Naguib, M. Kurtoglu, V. Presser, J. Lu, J.J. Niu, M. Heon, L. Hultman, Y. Gogotsi, M.W. Barsoum, Two-Dimensional Nanocrystals Produced by Exfoliation of Ti_3AlC_2, Advanced Materials, 23 (2011) 4248-4253.

[2] M. Naguib, O. Mashtalir, J. Carle, V. Presser, J. Lu, L. Hultman, Y. Gogotsi, M.W. Barsoum, Two-Dimensional Transition Metal Carbides, Acs Nano, 6 (2012) 1322-1331.

[3] Q. Tang, Z. Zhou, P. Shen, Are MXenes promising anode materials for Li ion batteries? Computational studies on electronic properties and Li storage capability of Ti_3C_2 and $Ti_3C_2X_2$ (X = F, OH) monolayer, J Am Chem Soc, 134 (2012) 16909-16916.

[4] D. Rao, L. Zhang, Y. Wang, Z. Meng, X. Qian, J. Liu, X. Shen, G. Qiao, R. Lu, Mechanism on the Improved Performance of Lithium Sulfur Batteries with MXene-Based Additives, Journal of

Physical Chemistry C, 121 (2017) 11047-11054.

[5] X. Tang, D. Zhou, P. Li, X. Guo, B. Sun, H. Liu, K. Yan, Y. Gogotsi, G. Wang, MXene-Based Dendrite-Free Potassium Metal Batteries, Advanced Materials, 32 (2020).

[6] F.W. Ming, H.F. Liang, G. Huang, Z. Bayhan, H.N. Alshareef, MXenes for Rechargeable Batteries Beyond the Lithium-Ion, Advanced Materials, 33 (2021).

[7] G. Gao, A.P. O'Mullane, A. Du, 2D MXenes: A New Family of Promising Catalysts for the Hydrogen Evolution Reaction, ACS Catalysis, 7 (2016) 494-500.

[8] K.R.G. Lim, A.D. Handoko, L.R. Johnson, X. Meng, M. Lin, G.S. Subramanian, B. Anasori, Y. Gogotsi, A. Vojvodic, Z.W. Seh, 2H-MoS_2 on Mo_2CT_x MXene Nanohybrid for Efficient and Durable Electrocatalytic Hydrogen Evolution, ACS Nano, 14 (2020) 16140-16155.

[9] Z.W. Seh, K.D. Fredrickson, B. Anasori, J. Kibsgaard, A.L. Strickler, M.R. Lukatskaya, Y. Gogotsi, T.F. Jaramillo, A. Vojvodic, Two-Dimensional Molybdenum Carbide (MXene) as an Efficient Electrocatalyst for Hydrogen Evolution, ACS Energy Letters, 1 (2016) 589-594.

[10] Z. Wu, L. Wei, S. Tang, Y. Xiong, X. Qin, J. Luo, J. Fang, X. Wang, Recent Progress in $Ti_3C_2T_X$ MXene-Based Flexible Pressure Sensors, Acs Nano, 15 (2021) 18880-18894.

[11] D.H. Ho, Y.Y. Choi, S.B. Jo, J.-M. Myoung, J.H. Cho, Sensing with MXenes: Progress and Prospects, Advanced Materials, 33 (2021).

[12] Y. Wang, Y. Yue, F. Cheng, Y. Cheng, B. Ge, N. Liu, Y. Gao, $Ti_3C_2T_x$ MXene-Based Flexible Piezoresistive Physical Sensors, Acs Nano, 16 (2022) 1734-1758.

[13] C. Liu, S. Hao, X. Chen, B. Zong, S. Mao, High Anti-Interference $Ti_3C_2T_x$ MXene Field-Effect-Transistor-Based Alkali Indicator, Acs Applied Materials & Interfaces, 12 (2020) 32970-

32978.

[14] B. Zong, Q. Xu, S. Mao, Single-Atom Pt-Functionalized $Ti_3C_2T_x$ Field-Effect Transistor for Volatile Organic Compound Gas Detection, ACS Sensors, 7 (2022) 1874-1882.

[15] B. Xu, M. Zhu, W. Zhang, X. Zhen, Z. Pei, Q. Xue, C. Zhi, P. Shi, Ultrathin MXene-Micropattern-Based Field-Effect Transistor for Probing Neural Activity, Advanced Materials, 28 (2016) 3333-3339.

[16] A.V. Mohammadi, J. Rosen, Y. Gogotsi, The world of two-dimensional carbides and nitrides (MXenes), Science, 372 (2021) 1165-+.

[17] C.F.J. Zhang, S. Pinilla, N. McEyoy, C.P. Cullen, B. Anasori, E. Long, S.H. Park, A. Seral-Ascaso, A. Shmeliov, D. Krishnan, C. Morant, X.H. Liu, G.S. Duesberg, Y. Gogotsi, V. Nicolosi, Oxidation Stability of Colloidal Two-Dimensional Titanium Carbides (MXenes), Chemistry of Materials, 29 (2017) 4848-4856.

[18] H.H. Shi, P.P. Zhang, Z.C. Liu, S. Park, M.R. Lohe, Y.P. Wu, A.S. Nia, S. Yang, X.L. Feng, Ambient-Stable Two-Dimensional Titanium Carbide (MXene) Enabled by Iodine Etching, Angewandte Chemie-International Edition, 60 (2021) 8689-8693.

[19] F.C. Cao, Y. Zhang, H.Q. Wang, K. Khan, A.K. Tareen, W.J. Qian, H. Zhang, H. Agren, Recent Advances in Oxidation Stable Chemistry of 2D MXenes, Advanced Materials, 34 (2022).

[20] T. Habib, X.F. Zhao, S.A. Shah, Y.X. Chen, W.M. Sun, H. An, J.L. Lutkenhaus, M. Radovic, M.J. Green, Oxidation stability of $Ti_3C_2T_x$ MXene nanosheets in solvents and composite films, Npj 2d Materials and Applications, 3 (2019).

[21] S.H. Huang, V.N. Mochalin, Hydrolysis of 2D Transition-Metal Carbides (MXenes) in

Colloidal Solutions, Inorganic Chemistry, 58 (2019) 1958-1966.

[22] X.F. Zhao, D.E. Holta, Z.Y. Tan, J.H. Oh, I.J. Echols, M. Anas, H.X. Cao, J.L. Lutkenhaus, M. Radovic, M.J. Green, Annealed $Ti_3C_2T_z$ MXene Films for Oxidation-Resistant Functional Coatings, ACS Applied Nano Materials, 3 (2020) 10578-10585.

[23] J. Deng, J.A. Iniguez, C. Liu, Electrocatalytic Nitrogen Reduction at Low Temperature, Joule, 2 (2018) 846-856.

[24] Y.Y. Jiang, P.J. Ni, C.X. Chen, Y.Z. Lu, P. Yang, B. Kong, A. Fisher, X. Wang, Selective Electrochemical H_2O_2 Production through Two-Electron Oxygen Electrochemistry, Advanced Energy Materials, 8 (2018).

[25] Y. Okamoto, First-principles molecular dynamics simulation of O_2 reduction on ZrO_2 (1 1 1) surface, Applied Surface Science, 255 (2008) 3434-3441.

[26] S. Bawari, T.N. Narayanan, J. Mondal, Atomistic Elucidation of Sorption Processes in Hydrogen Evolution Reaction on a van der Waals Heterostructure, Journal of Physical Chemistry C, 122 (2018) 10034-10041.

[27] Y.Y.L. Sun, C. Zhan, P.R.C. Kent, M. Naguib, Y. Gogotsi, D.E. Jiang, Proton Redox and Transport in MXene-Confined Water, Acs Applied Materials & Interfaces, 12 (2020) 763-770.

[28] T. Wu, P.R.C. Kent, Y. Gogotsi, D.E. Jiang, How Water Attacks MXene, Chemistry of Materials, 34 (2022) 4975-4982.

[29] L. Zhang, J. Han, H. Wang, R. Car, W. E, Deep Potential Molecular Dynamics: A Scalable Model with the Accuracy of Quantum Mechanics, Physical Review Letters, 120 (2018) 143001.

[30] L.F. Zhang, J.Q. Han, H. Wang, W.A. Saidi, R. Car, W.N. E, End-to-end Symmetry Preserving

Inter-atomic Potential Energy Model for Finite and Extended Systems, 32nd Conference on Neural Information Processing Systems (NIPS), Montreal, CANADA, 2018.

[31] L.F. Zhang, D.Y. Lin, H. Wang, R. Car, W.N. E, Active learning of uniformly accurate interatomic potentials for materials simulation, Physical Review Materials, 3 (2019).

[32] L. Zhang, H. Wang, R. Car, W. E, Phase Diagram of a Deep Potential Water Model, Phys Rev Lett, 126 (2021) 236001.

[33] J. Zeng, L. Cao, M. Xu, T. Zhu, J.Z.H. Zhang, Complex reaction processes in combustion unraveled by neural network-based molecular dynamics simulation, Nat Commun, 11 (2020) 5713.

[34] Y.Z. Zhang, H.D. Wang, W.J. Chen, J.Z. Zeng, L.F. Zhang, H. Wang, E. Weinan, DP-GEN: A concurrent learning platform for the generation of reliable deep learning based potential energy models, Computer Physics Communications, 253 (2020).

[35] M.F. Calegari Andrade, H.Y. Ko, L. Zhang, R. Car, A. Selloni, Free energy of proton transfer at the water-TiO_2 interface from ab initio deep potential molecular dynamics, Chem Sci, 11 (2020) 2335-2341.

[36] H. Wang, L.F. Zhang, J.Q. Han, W.N. E, DeePMD-kit: A deep learning package for many-body potential energy representation and molecular dynamics, Computer Physics Communications, 228 (2018) 178-184.

[37] S.S. Batsanov, Van der Waals radii of elements, Inorganic Materials, 37 (2001) 871-885.

[38] B. Cordero, V. Gomez, A.E. Platero-Prats, M. Reves, J. Echeverria, E. Cremades, F. Barragan, S. Alvarez, Covalent radii revisited, Dalton Transactions, DOI 10.1039/b801115j(2008) 2832-2838.

[39] O. Markovitch, H. Chen, S. Izvekov, F. Paesani, G.A. Voth, N. Agmon, Special Pair Dance and Partner Selection: Elementary Steps in Proton Transport in Liquid Water, The Journal of Physical Chemistry B, 112 (2008) 9456-9466.

[40] S. Doo, A. Chae, D. Kim, T. Oh, T.Y. Ko, S.J. Kim, D.-Y. Koh, C.M. Koo, Mechanism and Kinetics of Oxidation Reaction of Aqueous $Ti_3C_2T_x$ Suspensions at Different pHs and Temperatures, ACS Applied Materials & Interfaces, 13 (2021) 22855-22865.

[41] A. Lipatov, M. Alhabeb, M.R. Lukatskaya, A. Boson, Y. Gogotsi, A. Sinitskii, Effect of Synthesis on Quality, Electronic Properties and Environmental Stability of Individual Monolayer Ti3C2 MXene Flakes, Advanced Electronic Materials, 2 (2016).

[42] X. Wang, Z. Wang, J. Qiu, Stabilizing MXene by Hydration Chemistry in Aqueous Solution, 60 (2021) 26587-26591.

[43] G. Kresse, J. Furthmiiller, Efficiency of ab-initio total energy calculations for metals and semiconductors using a plane-wave basis set, Computational Materials Science, 6 (1996) 15-50.

[44] G. Kresse, D.J.P.r.b. Joubert, From ultrasoft pseudopotentials to the projector augmented-wave method, Physical Review B, 59 (1999) 1758.

[45] J.P. Perdew, K. Burke, M.J.P.r.l. Ernzerhof, Generalized gradient approximation made simple, Phys Rev Lett, 77 (1996) 3865.

[46] S. Grimme, J. Antony, S. Ehrlich, H.J.T.J.o.c.p. Krieg, A consistent and accurate ab initio parametrization of density functional dispersion correction (DFT-D) for the 94 elements H-Pu, Journal of Chemical Physics, 132 (2010) 154104.

[47] S. Grimme, S. Ehrlich, L. Goerigk, Effect of the damping function in dispersion corrected

density functional theory, J Comput Chem, 32 (2011) 1456-1465.

[48] S. Plimpton, Fast Parallel Algorithms for Short-Range Molecular Dynamics, Journal of Computational Physics, 117 (1995) 1-19.